JPE 15-5-3

http://dx.doi.org/10.6113/JPE.2015.15.5.1168
ISSN(Print): 1598-2092 / ISSN(Online): 2093-4718

Scheme to Improve the Line Current Distortion of PFC Using a Predictive Control Algorithm

Dae Joong Kim*, Jin-Hyuk Park*, and Kyo-Beum Lee†

*,†Department of Electrical and Computer Engineering, Ajou University, Suwon, Korea

Abstract

This paper presents a scheme to improve the line current distortion of power factor corrector (PFC) topology at the zero crossing point using a predictive control algorithm in both the continuous conduction mode (CCM) and discontinuous conduction mode (DCM). The line current in single-phase PFC topology is distorted at the zero crossing point of the input AC voltage because of the characteristic of the general proportional integral (PI) current controller. This distortion degrades the line current quality, such as the total harmonic distortion (THD) and the power factor (PF). Given the optimal duty cycle calculated by estimating the next state current in both the CCM and DCM, the proposed predictive control algorithm has a fast dynamic response and accuracy unlike the conventional PI current control method. These advantages of the proposed algorithm lower the line current distortion of PFC topology. The proposed method is verified through PSIM simulations and experimental results with 1.5 kW bridgeless PFC (BLPFC) topology.

Key words: Bridgeless PFC (BLPFC), Digital control, Power factor corrector (PFC), Predictive control, Zero crossing distortion

I. INTRODUCTION

A power factor corrector (PFC) is a power converter controlled in such a manner that the line current has a high power factor (PF). Unlike diode rectifiers, PFC converters have been widely used in AC-to-DC power supply topologies because of their advantages of unit PF and lower line current distortion. Most PFC converters are controlled by the proportional integral (PI) controller. Many topologies are employed in PFC converters, and the boost converter type topology is a popular method with a simple structure [1]. However, the bridgeless PFC (BLPFC) has recently gained considerable research interest because of its higher efficiency compared with the conventional boost type PFC [2], [3]. The boost converter-type PFC is shown in Fig. 1, whereas the BLPFC is shown in Fig. 2. The BLPFC consists of two switches and two diodes without the diode rectifier bridge as its name implies. Given the elimination of the diode rectifier, the BLPFC has a high efficiency [4]-[7].

However, the line current of the PFC converter contains some distortion at the zero crossing point. This problem becomes more serious as the system power decreases and its line frequency increases. In particular, this distortion has been considered an important issue for most low-power applications. The main reasons for this distortion are as follows. The first reason is the dynamic response of the PI controller. Given the bandwidth of the PI current controller, its dynamic response is considerably slow. The line current is distorted because the error of the PI controller is considerably large, especially at the zero crossing point. The second reason for this distortion is the discontinuous conduction mode (DCM) operation of the PFC converter. Given the reason indicated in [8], [9], the PFC converter operates in the DCM near the zero crossing point of the input AC voltage. The line current cannot follow the reference current in this DCM interval, which results in line current distortion [10]. A controller with a fast dynamic response is required to lower this distortion [11]. Active research on predictive control has recently been conducted to obtain fast dynamic response of the control [12]-[19].

This paper presents a scheme to lower the line current distortion of PFC topology at the zero crossing point using a predictive control algorithm. The proposed predictive control algorithm predicts the current of the next state from the current of the present state in both the continuous conduction

Manuscript received Feb. 6, 2015; accepted Apr. 17, 2015
Recommended for publication by Associate Editor Joung-Hu Park.
†Corresponding Author: kyl@ajou.ac.kr
Tel: +82-31-219-2376, Fax: +81-31-212-9531, Ajou University
*Dept. of Electrical and Computer Eng., Ajou University, Korea

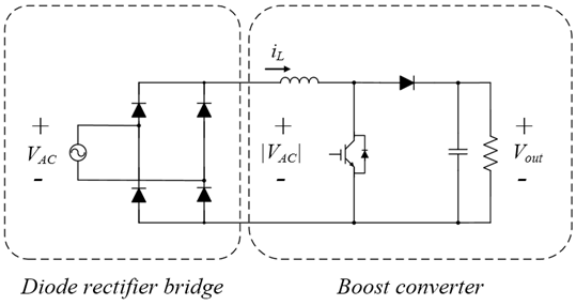

Fig. 1. Boost converter-type PFC topology.

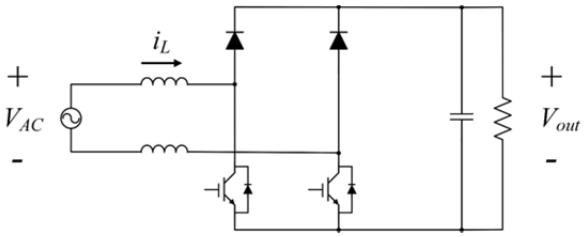

Fig. 2. BLPFC topology.

mode (CCM) and DCM. Given the optimal duty cycle obtained by minimizing the error between the reference and estimated currents, the proposed algorithm has a fast dynamic response unlike the conventional PI control method. The line current distortion at the zero crossing point can be lowered by applying the proposed method. The proposed method is verified with PSIM simulations and experimental results with the 1.5 kW BLPFC topology.

II. Conventional PFC Topology

A. PFC Topology with the Conventional PI Control Method

Fig. 1 shows a traditional boost converter-type PFC topology, whereas Fig. 2 shows a BLPFC topology. The boost converter-type PFC topology comprises a diode rectifier and boost converter. The BLPFC topology has higher efficiency than the boost-type PFC topology because the BLPFC topology does not employ a diode rectifier. The BLPFC topology can therefore decrease the conduction loss of switching devices unlike the boost-type PFC converter.

The BLPFC operation in a positive cycle of the input AC voltage is represented in Fig. 3. S_1 and S_2 are switches, whereas D_1 and D_2 are diodes. The BLPFC operates similar to a boost converter that uses S_1 and D_1 when the input AC voltage becomes positive. Fig. 3(a) shows that S_1 is turned ON and the current flows from the input V_{AC} through the inductor L to store energy. When S_1 is turned OFF as shown in Fig. 3 (b), the energy in L is released as current flows through D_1 through the load and returns to V_{AC} through the freewheeling diode of S_2. Events in the second half of the period repeat in the same manner as in the first half that uses S_2 and D_2.

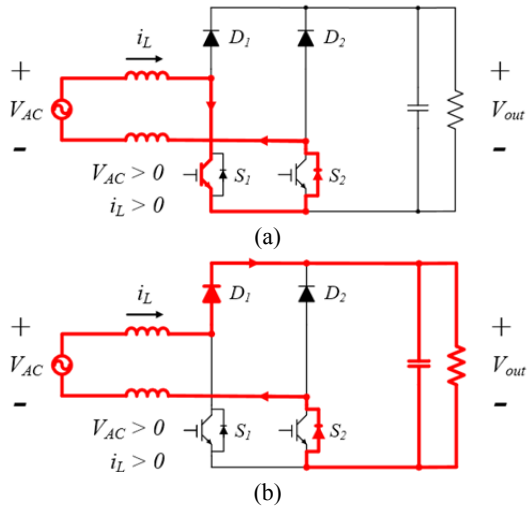

Fig. 3. Current flow of BLPFC in a positive cycle of the input AC voltage. (a) Switch ON interval, and (b) Switch OFF interval.

Although PFC converters have many topologies, most of them have two PI control loops. The inner current loop maintains the form of the sinusoidal current on the basis of the shape of the input AC voltage. Determining the accurate form of the input AC voltage $|sin\omega t|$ is important to achieve the PFC objective. $|sin\omega t|$ can be obtained simply by sensing the input AC voltage, but this method is too weak for the noise component, especially around the zero crossing point of the input AC voltage. Thus, the Phase Locked Loop (PLL) can be used to obtain the accurate $|sin\omega t|$ [20]-[21]. We can determine the magnitude, phase, and frequency of the input AC voltage through the PLL. Given the use of PLL, the current controller can accurately control the line current in the form of the input AC_voltage, including the zero crossing point of the input AC voltage. The outer voltage control loop maintains the required DC voltage and determines the amplitude of the current from the output voltage feedback. The block diagram of the control scheme, which includes the PI controller for the general PFC, is shown in Fig. 4. The inner current loop should have a high bandwidth unlike the outer voltage control loop. The transfer function of the inductor current system can be expressed as follows:

$$G_{id}(s) = \frac{i_L(s)}{d(s)} = \frac{\frac{V_{out}}{L} \cdot s}{s^2 + \frac{1}{L \cdot C_{out}}} \quad (1)$$

where L is the inductance of the PFC, and C_{out} is the output capacitance [22].

The transfer function of the PI controller can be expressed as follows:

$$G_{PI}(s) = K_p + \frac{K_i}{s} \quad (2)$$

where K_p is the proportional gain, and K_i is the integral gain of the PI controller. The current control block diagram is

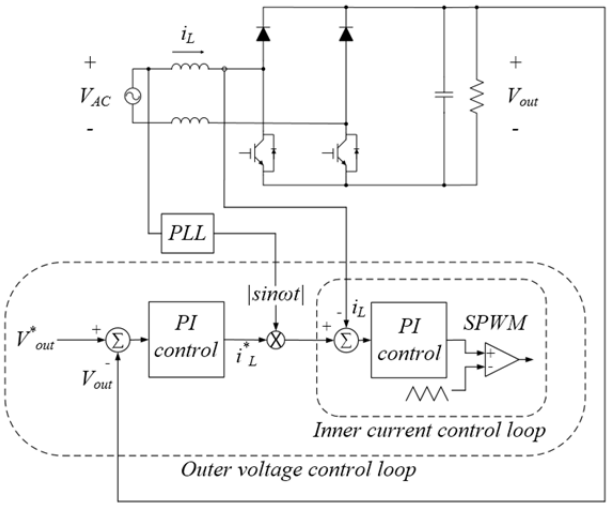

Fig. 4. Block diagram of the general PFC control.

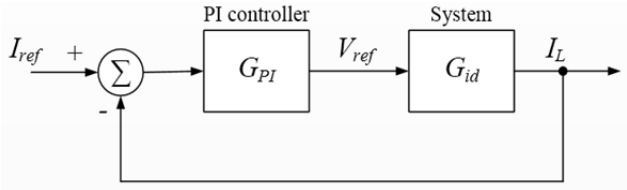

Fig. 5. Control diagram that includes the PI controller and system.

shown in Fig. 5. The closed loop transfer function that considers the PI controller can be expressed as follows:

$$T_{CL} = \frac{G_{id} \cdot G_{PI}}{1 + G_{id} \cdot G_{PI}} = \frac{\frac{V_{out}K_p}{L}s + \frac{V_{out}K_i}{L}}{s^2 + \frac{V_{out}K_p}{L}s + \frac{V_{out}K_i}{L} + \frac{1}{LC}}. \quad (3)$$

The bandwidth and gain of the PI current controller are selected by the stability criterion using the closed loop transfer function of the current controller and bode plot to stabilize the system. This bandwidth is also generally determined to be 1/20 to 1/10 of the switching frequency because the controller with excessively large bandwidth is weak for the noise and disturbance.

B. Zero Crossing Distortion of the Conventional Method

Fig. 6 shows the line current distortion at the zero crossing point of the input AC voltage. This distortion has two main reasons. The first reason is the slow dynamic response of the PI current controller. As mentioned in the previous section, the PI controller has a determined bandwidth that depends on the switching frequency of the system. This bandwidth limits the fast dynamic response of the PI current controller. Given the characteristic of the PI current controller, its error becomes larger than usual in the vicinity of the zero crossing point where the polarity of the input AC voltage changes. Moreover, the PI controller, which is suitable for controlling the DC component, cannot control the AC component properly. Thus, this error of the PI controller further affects

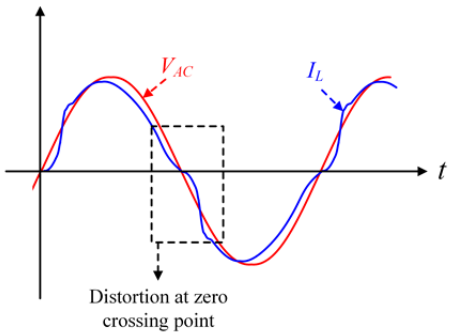

Fig. 6. Zero crossing distortion of the filtered line current.

the line current distortion. The second reason for this distortion is the mode conversion of the PFC converter. The PFC converter operation can be divided into two modes, the CCM and DCM. The line current has a leading phase relative to the input AC voltage at the zero crossing point because the PI current controller has a slow dynamic response [8]. When the line current decreases to zero from a positive value, the input AC voltage remains positive and the PFC converter operates in the DCM [9]. Similarly, when the line current decreases to zero from a negative value, the input AC voltage remains negative and the PFC converter operates in the DCM. The sensing current in the digital control is generally different from the average current in the DCM. Therefore, the digital PI current controller in this DCM operation interval cannot control the average current and intensifies the line current distortion. The distortion aggravates the line current quality such as the total harmonic distortion (THD) and PF. This distortion becomes more severe in a low-power system because the operating duration in the DCM is large when a small current flows.

III. Proposed Algorithm for Distortion Reduction

This paper presents a scheme to decrease the line current distortion at the zero crossing point using a predictive control algorithm. The proposed predictive control algorithm has a fast dynamic response unlike the conventional PI current controller because the optimal duty is calculated by predicting the next state current using the value of the slope of the inductor current. However, the calculation method should vary depending on the mode of the PFC converter because the line current shape is different depending on the mode. Thus, this paper presents a predictive current control algorithm in the CCM and DCM. The equivalent circuit of the PFC converter is shown in Figs. 7 and 8. Fig. 7 shows the current flow of the PFC converter during the switch ON time, whereas Fig. 8 shows the current flow of the PFC converter during the switch OFF time.

During the switch ON time T_{on}, the voltage equation is expressed as follows:

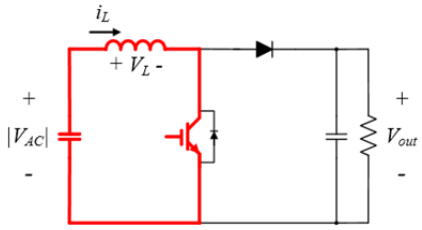

Fig. 7. Current flow of the PFC converter during the switch ON time.

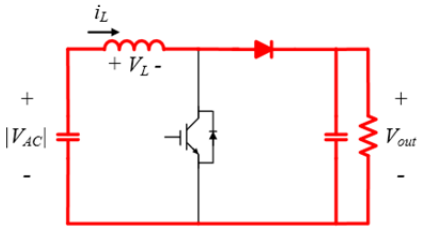

Fig. 8. Current flow of the PFC converter during the switch OFF time.

$$|V_{AC}| - V_L = |V_{AC}| - L\frac{di_L}{dt} = 0. \quad (4)$$

Rearranging Equation (4), the slope of the inductor current in T_{on} can be determined as follows:

$$S_{on} = \frac{di_L}{dt} = \frac{|V_{AC}|}{L}. \quad (5)$$

This inductor current slope has a positive value in T_{on} because the absolute value of the input AC voltage $|V_{AC}|$ is always positive. During the switch OFF time T_{off}, the voltage equation is similarly expressed as follows:

$$|V_{AC}| = V_{out} + V_L = V_{out} + L\frac{di_L}{dt}. \quad (6)$$

From Equation (6), the slope of the inductor current can be obtained as follows:

$$S_{off} = \frac{di_L}{dt} = \frac{|V_{AC}| - V_{out}}{L}. \quad (7)$$

This inductor current slope has a negative value in T_{off} because the value of the output voltage is always larger than $|V_{AC}|$ in the steady state.

The accurate instantaneous value of V_{AC} is required to obtain the accurate slope of the line current because the V_{out} can be seen as a constant value in the steady state. The values of the voltage and current are obtained simultaneously by sampling in the middle point of the rising edge of the inductor current at every switching cycle. Given that the value of the voltage is used to calculate the slope of the line current, the accurate slope of the line current at the time when the sensing is performed can be obtained. The proposed method also has a problem of one-cycle delay in the control similar to other digital control methods. However, the problem of one-cycle delay can be ignored in the control of low-power applications such as PFC converters unlike other cases because the low-power applications have a fast sampling frequency.

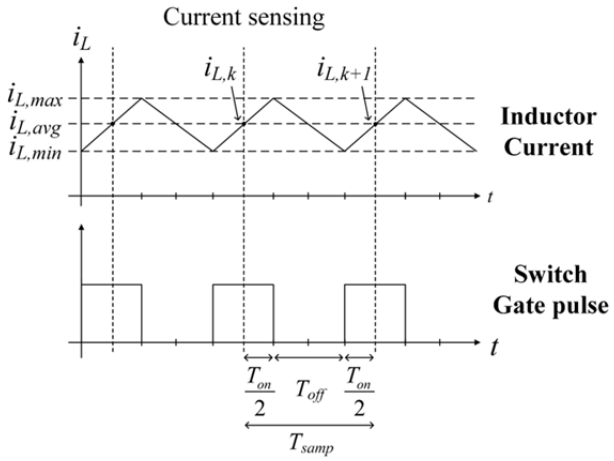

Fig. 9. Inductor current and gating pulse of the switch in the CCM steady state.

A. Calculation of the Optimal Duty for CCM Operation

Fig. 9 shows the inductor current and gating pulse of the switch in the CCM steady state. The average value of the inductor current in the CCM is the same as the sensing current. Given the inductor current of the current state $i_{L,k}$, the inductor current of the next state $i_{L,k+1}$ can be estimated using the slope of the inductor current, which is given by Equations (5) and (7). The estimated inductor current of the next state can be obtained as follows:

$$i_{L,k+1} = i_{L,k} + S_{on} \cdot T_{on} + S_{off} \cdot \left(T_{samp} - T_{on}\right) \quad (8)$$

where T_{samp} is the sampling period, which is the sum of T_{on} and T_{off}.

The difference i_{err} between the reference current i^*_L and $i_{L,k+1}$ is expressed as follows:

$$i_{err} = i^*_L - i_{L,k+1}. \quad (9)$$

Assume that this error in Equation (9) is zero, then Equation (10) can be obtained from Equations (8) and (9).

$$\begin{aligned} i_{err} &= i^*_L - i_{L,k+1} \\ &= i^*_L - i_{L,k} - S_{on} \cdot T_{on} - S_{off} \cdot \left(T_{samp} - T_{on}\right) = 0 \end{aligned}. \quad (10)$$

Rearranging Equation (10), T_{on} can be calculated as follows:

$$T_{on} = \frac{i^*_L - i_{L,k} - S_{off} \cdot T_{samp}}{S_{on} - S_{off}}. \quad (11)$$

Using Equation (11), the optimal duty cycle to set i_{err} to zero in the CCM of the PFC converter can be obtained as follows:

$$Duty = \frac{T_{on}}{T_{samp}}. \quad (12)$$

B. Calculation of the Optimal Duty for DCM Operation

Fig. 10 shows the inductor current and gating pulse of the switch in the DCM steady state. The DCM operation has the characteristic of the sensing current being different from the average value of the inductor current. Thus, the average

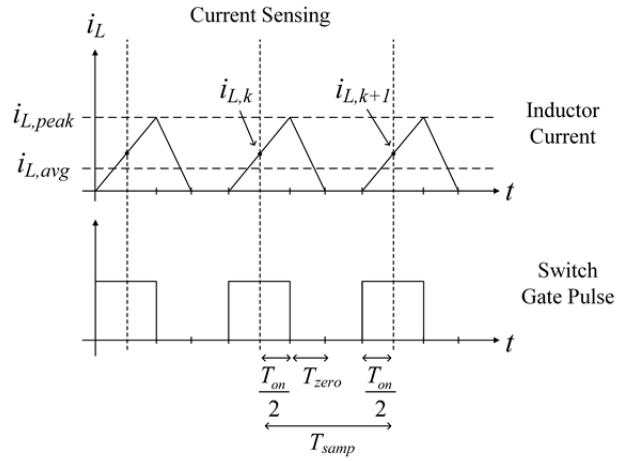

Fig. 10. Inductor current and gating pulse of the switch in the DCM steady state.

inductor current cannot follow to the reference current when the CCM method is applied to the DCM. Therefore, a predictive control method for the DCM is proposed.

Using a similar method of prediction to that used for the CCM, the average inductor current in the DCM can be predicted. The peak inductor current $i_{L,peak}$ is the increased value from zero for T_{on}.

$$i_{L,peak} = S_{on} \cdot T_{on} \tag{13}$$

T_{zero} is the time that the current reaches zero from $i_{L,peak}$. The relationship between $i_{L,peak}$ and T_{zero} can be expressed as follows:

$$i_{L,peak} = S_{on} \cdot T_{on} = -S_{off} \cdot T_{zero} . \tag{14}$$

T_{zero} can be obtained using Equation (14).

$$T_{zero} = -\frac{S_{on} \cdot T_{on}}{S_{off}} . \tag{15}$$

Unlike the CCM, the average value of the inductor current is different from the intermediate value of the current when operating in the DCM as previously mentioned. Therefore, the estimated average value of the inductor current in the DCM should be calculated.

Using the current integration, the estimated average value of the inductor current, $i_{L,avg,n+1}$, can be obtained as follows

$$i_{L,avg,n+1} = \frac{i_{L,peak} \cdot \left(T_{on} + T_{zero}\right)}{2 \cdot T_{samp}} . \tag{16}$$

The difference i_{err} between i^*_L and $i_{L,avg,n+1}$ is expressed as follows:

$$i_{err} = i_L^* - i_{L,avg,n+1} . \tag{17}$$

If i_{err} is assumed to be zero, Equation (18) is obtained from Equation (14) to (17).

$$i_{err} = i_L^* - \frac{\left(S_{on} \cdot T_{on}\right) \cdot \left(T_{on} - \left(\frac{S_{on} \cdot T_{on}}{S_{off}}\right)\right)}{2 \cdot T_{samp}} = 0 . \tag{18}$$

T_{on} can be expressed as follows:

TABLE I
PSIM SIMULATION AND EXPERIMENT PARAMETERS

Input AC voltage	Magnitude	220 V_{rms}
	Frequency	60 Hz
Output Voltage		380 V
Rated Power		1.5 kW
AC Voltage Side Inductance		2.4 mH
Output Capacitance		4080 μF
Switching Frequency		16.67 kHz
Sampling Period		60 μs
Bandwidth of PI controller		10000 rad/s

$$T_{on} = \sqrt{\frac{2 \cdot i_L^* \cdot T_{samp}}{S_{on} \cdot (1 - \frac{S_{on}}{S_{off}})}} . \tag{19}$$

Using Equation (19), the optimal duty for setting i_{err} to zero in the DCM of the PFC converter can be obtained as follows:

$$Duty = \frac{T_{on}}{T_{samp}} . \tag{20}$$

IV. SIMULATION RESULTS

The simulation was performed using PSIM software to verify the validity of the proposed algorithm. The simulation parameters are listed in Table I. The output DC voltage in all cases is controlled to 380 V.

Figs. 11 and 12 show the line current of the PFC topology when the conventional PI current controller is used. Fig. 11 shows the line current in the 375 W (25% of the rated power) operation. The distortion of the line current can be seen over almost the entire interval. As mentioned in the previous section, the distortion becomes more serious in a low-power system because of the wide operating interval in the DCM.

Fig. 12 shows the line current in the 1.5 kW (100% of the rated power) operation. The line current distortion is not highlighted in the CCM. However, the line current can be confirmed as clearly distorted in the DCM, including at the zero crossing point.

Figs. 13 and 14 show the performance of the proposed algorithm for PFC topology. Fig. 13 shows the performance in the 375 W (25% of the rated power) operation. Comparing Fig. 13 to Fig. 11 shows that the distortion has decreased. This reduction in the distortion is achieved because the proposed method can control the average current by estimating the current for the CCM and DCM.

Fig. 14 shows the performance in the 1.5 kW (100% of the rated power) operation. The line current over the entire interval can follow the reference current accurately without

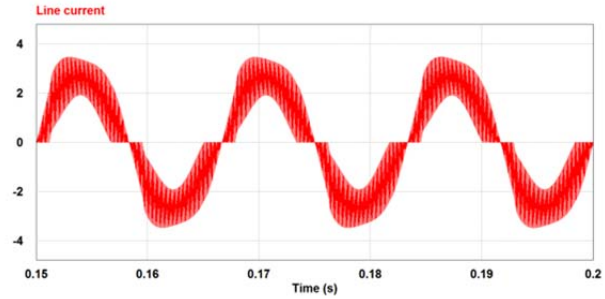

Fig. 11. Simulation result of line current for 375 W (25% of the rated power) operation when using the PI controller.

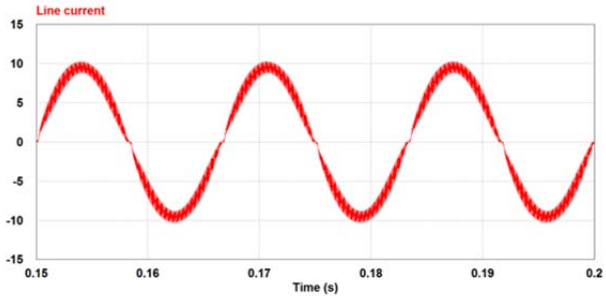

Fig. 12. Simulation result of line current for 1.5 kW (100% of the rated power) operation when using the PI controller.

distortion and delay because of the fast dynamic response of the proposed method. As the foregoing simulation results show, the proposed algorithm lowers the distortion of the line current at the zero crossing point.

V. Experimental Results

The experiments were conducted using the 1.5 kW BLPFC set and TMS320F28335 DSP controller as shown in Fig. 15 to verify the proposed predictive control algorithm. The precise power meter YOKOGAWA WT3000 was used to measure the PF and THD of the line current. The experiments were performed under the same condition as those for the PSIM simulations shown in Table I. Similar to the PSIM simulation, the output DC voltage is controlled to 380 V in all cases. In the experimental results, the input AC voltage is the actual grid voltage that includes some distortions.

The controller performance is influenced by the controller bandwidth in using the PI current controller. The stable bandwidth and stable gain of the PI current controller can be selected by the stability criterion using the closed loop transfer function of the controller and bode plot. In addition, the bandwidth of the PI current controller is also generally selected to be 1/20 to 1/10 of the switching frequency. Therefore, we can select the stable bandwidth of the PI current controller. When the bandwidth of the PI controller increases, the controller can control the current accurately. However, the controller becomes unstable when the PI current controller with a bandwidth larger than 10000 rad/s is

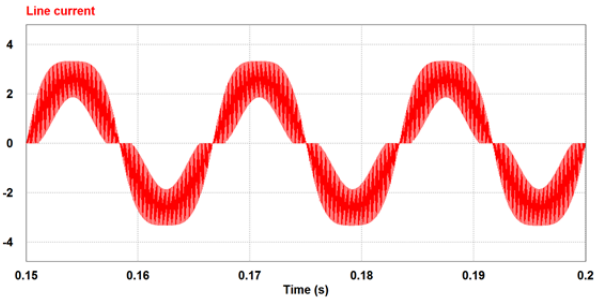

Fig. 13. Simulation result of line current for 375 W (25% of the rated power) operation when using the proposed algorithm.

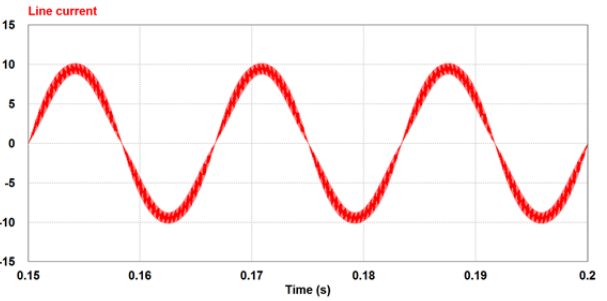

Fig. 14. Simulation result of line current for 1.5 kW (100% of the rated power) operation when using the proposed algorithm.

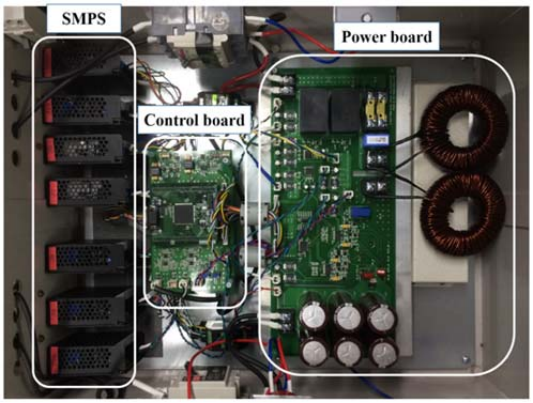

Fig. 15. Experimental setup of BLPFC topology.

used. Therefore, the PI current controller that has a bandwidth of 10000 rad/s is suitable for the current control. The proposed algorithm is compared with the current controller that has a bandwidth of 10000 rad/s to present the performance of the proposed algorithm.

Figs. 16 and 17 show the experimental results of PFC topology when the conventional PI current controller is used. Fig. 16 shows the experimental results for the 375 W (25% of the rated power) operation when using the PI controller. The line current is distorted over almost the entire interval and cannot follow the reference current because the PI controller has a slow dynamic response. In addition, the line current distortion becomes more serious in a low-power system because of the wide operating interval in the DCM.

Fig. 17 shows the experimental results for 1.5 kW (100% of the rated power) operation when using the PI controller. The line current is clearly distorted at the zero crossing point

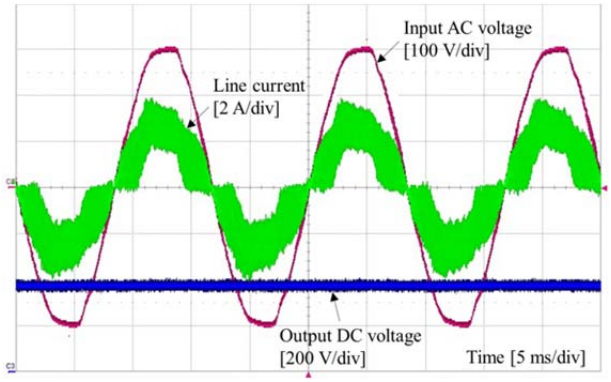

Fig. 16. Experimental results for 375 W (25% of the rated power) operation when using the PI controller.

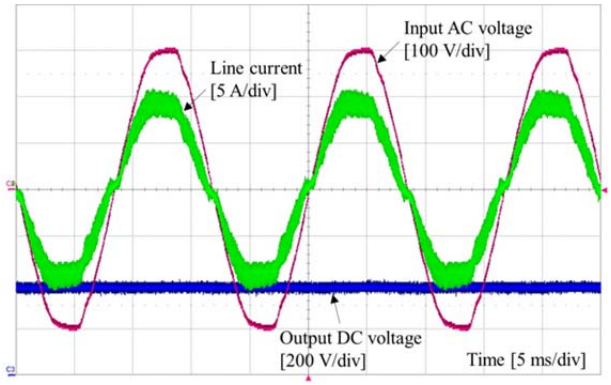

Fig. 17. Experimental results for 1.5 kW (100% of the rated power) operation when using the PI controller.

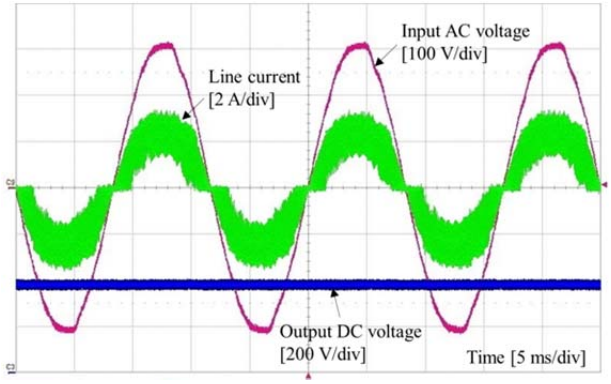

Fig. 18. Experimental results for 375 W (25% of the rated power) operation when using the proposed algorithm.

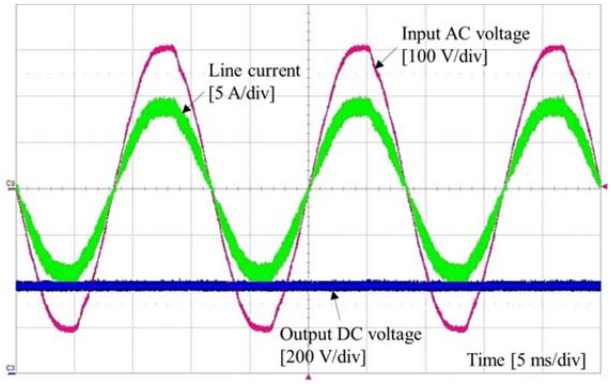

Fig. 19. Experimental results for 1.5 kW (100% of the rated power) operation when using the proposed algorithm.

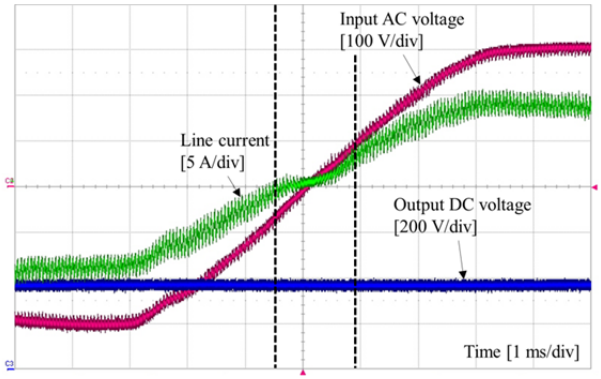

(a)

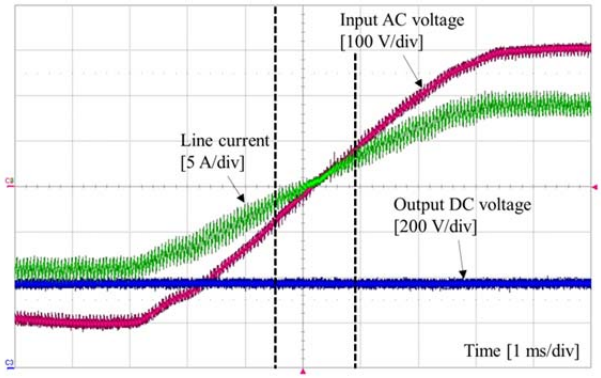

(b)

Fig. 20. Zero crossing interval of the input AC voltage for 1.5 kW (100% of the rated power) operation. (a) PI current controller, and (b) proposed controller.

of the input AC voltage. Similar to the result in Fig. 16, the line current cannot follow the reference current at the zero crossing point because the error of the PI controller becomes larger than usual at the zero crossing point, where the polarity of the input AC voltage changes.

Figs. 18 and 19 show the experimental results of PFC topology when the proposed predictive control algorithm is applied. Fig. 18 shows the performance in the 375 W (25% of the rated power) operation when using the proposed algorithm. Given the fast dynamic response of the proposed algorithm, the line current can follow the reference current without distortion and delay. The proposed algorithm can also control the average current using the estimation of the current for the CCM and DCM. Given these advantages of the algorithm, the distortion at the zero crossing point is lowered.

Fig. 19 shows the performance for the 1.5 kW (100% of the rated power) operation when using the proposed algorithm. The shape of the current becomes sinusoidal and the zero crossing distortion of the line current is apparently decreased compared with the result in Fig. 17. The line current can be controlled as required without the distortion using the proposed algorithm.

Fig. 20 shows the zero crossing interval of the input AC voltage for the 1.5 kW (100% of the rated power) operation. Fig. 20(a) shows the result of the PI controller, whereas Fig.

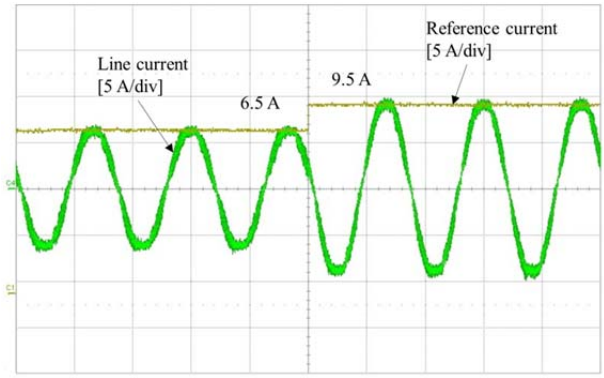

(a)

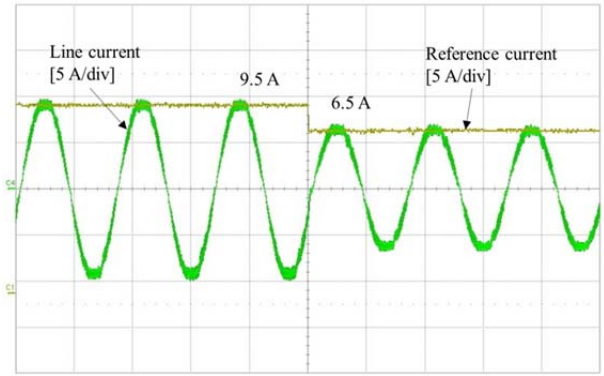

(b)

Fig. 21. Experimental results for the dynamic response of the proposed algorithm. (a) 6.5 A to 9.5 A, and (b) 9.5 A to 6.5 A.

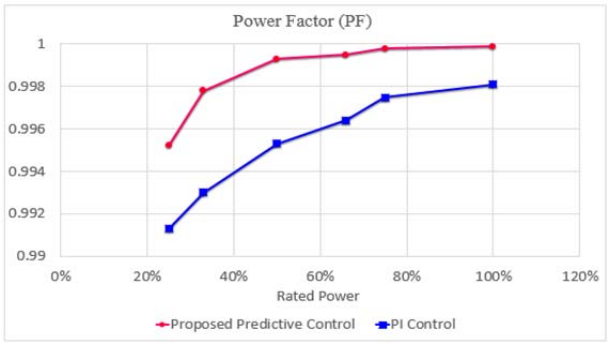

Fig. 22. PF of the line current when using the PI control and proposed predictive control.

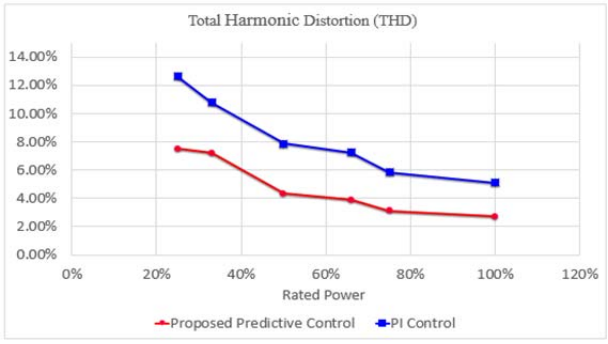

Fig. 23. THD of the line current when using the PI control and proposed predictive control.

20(b) shows the result of the proposed controller. In using the PI current controller as shown in Fig. 20(a), the line current can be confirmed to be distorted at the zero crossing point of the input AC voltage. However, the line current can be confirmed to be controlled in the sinusoidal form of the input AC voltage without distortion when using the proposed current controller as shown in Fig. 20(b).

Fig. 21 shows the experimental results for the dynamic response of the proposed algorithm. The reference current is changed during the operation to verify the dynamic performance of the proposed algorithm. The reference current is changed from 6.5 A to 9.5 A in Fig. 21(a) and 9.5 A to 6.5 A in Fig. 21(b). The line current follows the reference current immediately without the overshoot or undershoot in all cases because of the optimal duty of the proposed algorithm.

The PF of the line current when using the PI control and proposed predictive control are plotted in Fig. 22 against the ratio of the rated power. The PF of the PI control in the 25% rated power operation is 0.9913, whereas that of the proposed algorithm is 0.9952. The PF of the PI control in the 100% rated power operation is 0.9981, whereas that of the proposed algorithm is 0.9999. The PF measurement result shows that the PF of the proposed predictive control is always better than the PF of the PI control.

The THD of the line current when using the PI control and proposed predictive control are also shown in Fig. 23. The THD of the PI control for the 25% rated power operation is 12.63%, whereas that of the proposed algorithm is 7.5%. The THD of the PI control for the 100% rated power operation is 5.1%, whereas that of the proposed algorithm is 2.72%. The said results verify that the proposed algorithm improves the quality of the line current such as the THD and PF.

VI. Conclusion

A scheme to lower the line current distortion in PFC topology at the zero crossing point using a predictive control method in both the CCM and DCM was proposed in this paper. The proposed algorithm is based on predictive control. This proposed method has the advantage of lowering the line current distortion without the requirement of an additional circuit or complex control algorithm. Given the fast dynamic response of predictive control, the line current distortion can be lowered. Moreover, the line current can follow the reference current accurately over the entire interval because the proposed algorithm is divided into one for the CCM and another for the DCM. Therefore, the line current qualities, such as the PF and THD, are clearly improved when using the proposed method. The simulation and experimental results demonstrate that the proposed predictive control algorithm can effectively lower the line current distortion in PFC topology.

ACKNOWLEDGMENT

This work was supported by the Human Resources Development Program (No. 20134030200310) of the Korea Institute of Energy Technology Evaluation and Planning grant funded by the Korea Government Ministry of Knowledge Economy.

This research was also supported by the Basic Science Research Program through the National Research Foundation of Korea funded by the Ministry of Education (No. 2013R1A1A2A10006090)

REFERENCES

[1] K. P. Louganski and J. S. Lai, "Current phase lead compensation in single-phase PFC boost converters with a reduced switching frequency to line frequency ratio," *IEEE Trans. Power Electron.*, Vol. 22 , No. 1, pp. 113-119, Jan. 2007.

[2] B. Su and Z. Lu, "An interleaved totem-pole boost bridgeless rectifier with reduced reverse-recovery problems for power factor correction," *IEEE Trans. Power Electron.*, Vol. 25, No. 6, pp. 1406-1415, Jun. 2010.

[3] M. Mahdavi and H. Farzanehfard, "Zero-current-transition bridgeless PFC without extra voltage and current stress," *IEEE Trans. Ind. Electron.*, Vol. 56, No. 7, pp. 2540-2547, Jul. 2009.

[4] A. Fardoun, E. Ismail, A. Sabzali, and M. Al-Saffar, "Bridgeless resonant pseudo boost PFC rectifier," *IEEE Trans. Power Electron.*, Vol. 29, No. 11, pp. 5949-5960, Nov. 2014.

[5] L. Huber, Y. Jang, and M. M. Jovanovic, "Performance evaluation of bridgeless PFC boost rectifiers," *IEEE Trans. Power Electron.*, Vol. 23 , No. 3, pp. 1381-1390, May 2008.

[6] F. Musavi, W. Eberle, and W. G. Dunford, "A high-performance single phase bridgeless interleaved PFC converter for plug-in hybrid electric vehicle battery chargers," *IEEE Trans. Ind. Appl.*, Vol. 47, No. 4, pp. 1833-1843, Jul./Aug. 2011.

[7] W. Y. Choi, J. M. Kwon, E. H. Kim, J. J. Lee, and B. H. Kwon, "Bridgeless boost rectifier with low conduction losses and reduced diode reverse-recovery problems," *IEEE Trans. Ind. Electron.*, Vol. 54 , No. 2, pp. 769-780, Apr. 2007.

[8] J. Sun, "On the zero-crossing distortion in single-phase PFC converters," *IEEE Trans. Power Electron.*, Vol. 19, No. 3, pp. 685-692, May 2004.

[9] X. Qu and X. Ruan, "A scheme for improving input current zero-crossing distortion of single-phase power-factor- correction converters," in *Proc. PESC*, pp. 1-6, 2006.

[10] S. F. Lim and A. M. Khambadkone, "A simple digital DCM control scheme for boost PFC operating in both CCM and DCM," *IEEE Trans. Ind. Appl.*, Vol. 47, No. 4, pp. 1802-1812, Jul./Aug. 2011.

[11] J. H. Park, H. G. Jeong, and K. B. Lee, "Second order harmonics reduction technique using model predictive control for household energy storage systems," in *Proc. APEC*, pp. 3060-3065, 2014.

[12] T. Geyer, G. Papafotiou, and M. Morari, "Model predictive direct torque control–part I: Concept, algorithm, and analysis," *IEEE Trans. Ind. Electron.*, Vol. 56, No. 6, pp. 1916-1924, Jun. 2009.

[13] Y. Cho, K. B. Lee, J. H. Song, and Y. I. Lee, "Torque-ripple minimization and fast dynamic scheme for torque predictive control of permanent-magnet synchronous motors," *IEEE Trans. Power Electron.*, Vol. 30, No. 4, pp. 2182-2190, Apr. 2015.

[14] J. Gao, Q. T. Zheng, and F. Lin, "Improved deadbeat current controller with a repetitive -control-based observer for PWM rectifiers," *Journal of Power Electronics*, Vol. 11, No. 1, pp. 64-73, Jan. 2011.

[15] D. K. Choi and K. B. Lee, "Dynamic performance improvement of AC/DC PWM converter using model predictive direct power control set," *IEEE Trans. Ind. Electron.*, Vol. 62, No. 2, pp. 757-767, Feb. 2015.

[16] Y. He, J. Liu, J. Tang, Z. Wang, and Y. Zou, "Deadbeat control with a repetitive predictor for three-level active power filters," *Journal of Power Electronics*, Vol. 11, No. 4, pp. 583-590, Jul. 2011.

[17] G. Abad, M. A. Rodriguez, and J. Poza, "Two-level VSC based predictive direct torque control of the doubly fed induction machine with reduced torque and flux ripples at low constant switching frequency," *IEEE Trans. Power Electron.*, Vol. 23, No. 3, pp. 1050-1061, May 2008.

[18] E. Lee, K. B. Lee, Y. I. Lee, and J. H. Song, "High performance current controller for sparse matrix converter based on model predictive control," *Journal of Electrical Engineering & Technology*, Vol. 8, No. 5, pp. 1138-1145, Sep. 2013.

[19] D. K. Choi and K. B. Lee, "Model-based predictive control for interleaved multi-phase DC/DC converters," *Transactions of Korean Institute of Power Electronics(KIPE)*, Vol. 19, No. 5, pp. 415-421, Oct. 2014.

[20] Y. Cho, H. Mok, and J. S. Lai, "Analysis of the admittance component for digitally controlled single-phase bridgeless PFC converter," *Journal of Power Electronics*, Vol. 13, No. 4, pp. 600-608, Jul. 2013.

[21] S. B. Lim and S. C. Hong, "Hybrid UPS with energy storage system function," *Transactions of Korean Institute of Power Electronics(KIPE)*, Vol. 19, No. 3, pp. 266-275, Jun. 2014.

[22] H. G. Jeong and K. B. Lee, "A controller design for a stability improvement of an on-board battery charger," *Journal of Electrical Engineering & Technology*, Vol. 8, No. 4, pp. 951-958, Jul. 2013.

Dae Joong Kim received his B.S. in Electronic Engineering degree from Ajou University, Suwon, Korea in 2014. He is presently working toward his M.S. in Electronic Engineering degree at Ajou University. His current research interests include power conversion and grid-connected systems.

Jin-Hyuk Park received his B.S. in Electronic Engineering degree from Ajou University, Suwon, Korea in 2013. He is presently working toward his Ph.D. in Electronic Engineering degree at Ajou University. His current research interests include power conversion and grid-connected systems.

Kyo-Beum Lee received his B.S. and M.S. in Electrical and Electronic Engineering degrees from Ajou University, Suwon, Korea in 1997 and 1999, respectively. He received his Ph.D. in Electrical Engineering degree from Korea University, Seoul, Korea in 2003. He was part of the Institute of Energy Technology, Aalborg University, Aalborg Denmark from 2003 to 2006. He was part of the Division of Electronics and Information Engineering, Chonbuk National University, Jeonju, Korea from 2006 to 2007. He joined the Department of Electrical and Computer Engineering, Ajou University, Suwon, Korea in 2007. His current research interests include electric machine drives, electric vehicles, and renewable power generation.